Journal of Physics D: Applied Physics
*Submitted, February 21, 2007*

# Electrostatic Effects in the Gas-Phase Aggregation of Laser-Synthesized Zinc Oxide Nanoparticles

Masashi Matsumura*, Lorenzo Smith, Mevlut Bulut, and Renato P. Camata

*Department of Physics, University of Alabama at Birmingham*
*Birmingham, AL 35294, U.S.A.*

*Corresponding author: Department of Physics, University of Alabama at Birmingham,

CH 310, 1530 3$^{RD}$ AVE S, Birmingham, AL 35294-1170, U.S.A.

Tel.: 205-934-8143; Fax: 205-934-8042. *E-mail address*: matsu@uab.edu (M. Matsumura)

**ABSTRACT**

Gas-phase aggregation represents a significant problem in nanoparticle synthesis by vapor phase techniques. In this letter we show how gas-phase aggregation is inhibited by electrostatic effects in the synthesis of ZnO nanoparticles by laser evaporation in background gases. This technique, which allows high-purity and large-scale synthesis of nanoparticles of a variety of technologically important materials, produces a highly charged aerosol whose agglomeration is significantly retarded due to electrostatic repulsion between the particles. Direct measurements of the ZnO aerosol size distribution using a differential mobility analyzer are compared with the results of a simple particle dynamics model. The mean diameters of measured size distributions can only be explained if Coulomb corrections to the Brownian coagulation coefficients are included in the model.

**KEYWORDS:** Zinc oxide, Bimodal distribution, Laser ablation.

## 1. Introduction

Nanoparticles of the direct-gap semiconductor zinc oxide (ZnO) have attracted much attention recently because their increased surface area and quantum confinement effects allow tunability of optical [1], vibrational [2], and chemical properties [3], affording great freedom in the engineering of light emitting and memory devices [4,5], sensors [6], actuators [7], and other complex nanoscale systems [8]. Although many of these applications require high-purity ZnO nanoparticles with well controlled surfaces, most studies to date have employed particles synthesized by colloidal and flame pyrolysis methods that may present significant contamination problems [9,10]. High purity synthesis of ZnO nanoparticles has been reported by several chemical [11] and physical vapor methods [12] that nonetheless have the serious limitation of aggregation between nanoparticles in high throughput synthesis. Electrostatic interaction between charged particles in the gas phase has long been known to inhibit particle aggregation. However, the possibility of using this effect to control the aggregation of ZnO during gas phase synthesis has been the object of little investigation. In this letter we report on measurements of the size distribution of ZnO nanoparticles generated by laser ablation in background gases and on how an explanation of their aggregation behavior requires that electrostatic interactions be considered in the description of the problem.

## 2. Experimental

Gas-phase laser synthesis of ZnO nanoparticles was carried out using the experimental system illustrated in Fig. 1. The beam of a KrF excimer laser (248 nm wavelength; 10 Hz repetition rate) was focused to a spot with an area of 0.02 $cm^2$ and used

to ablate a rotating disk-shaped hot-pressed ZnO powder ceramic target (99.99% purity) mounted inside a windowed cell kept at a pressure of 1 Bar. The nanoparticles formed during ablation were entrained as an aerosol by a continuous flow of purified Ar gas (99.9995% purity) and after passing through a $^{85}Kr$ neutralizer where introduced into a differential mobility analyzer (DMA) operated in association with an aerosol electrometer for size distribution measurements. This measurement configuration has been described in detail elsewhere [13]. Briefly, the DMA with geometrical parameters $R_1$ = 25 mm, $R_2$ = 32 mm and $L$ = 18 mm, where $R_1$ and $R_2$ are the diameters of the inner and outer electrodes, and $L$ is the length of the classified region, was operated with an aerosol flow rate of 1 SLM (standard liter per minute) of Ar and 5 SLM of $N_2$ allowing measurements of the nanoparticle size distribution in the 1-60 nm range at 1 Bar. The flow rates were maintained constant during measurements by mass flow controllers. Inversion of the DMA mobility data was carried out using equilibrium charge distributions calculated according to Fuchs theory by the procedure described in Ref. 13.

**3. Size Distribution Measurements**

During ablation at low laser fluences (<2 J/cm$^2$), the gas-suspended nanoparticle populations consistently exhibited bimodal size distributions. A typical example is shown in the inset of Fig. 1 where the population produced using a pulse energy of 2.5 mJ was found to be well represented by a superposition of two log-normal distributions with geometric mean diameters of 14 nm and 39 nm, and geometric standard deviations of 1.55 and 1.65, respectively. Fig. 2 shows the effect of pulse laser energy on these bimodal size distributions. As the laser energy increases, the mean diameter of the “smaller-particle

mode" seems to shift to lower values whereas the "bigger-particle mode" remains largely unchanged. The relative concentrations of the two modes are also observed to change. Lower pulse energies lead to a population dominated by the smaller-particle mode while larger particles are predominant for higher pulsed energies.

The bimodal character of the observed size distributions can be explained by the coexistence of nucleation and accumulation processes during synthesis. This effect is illustrated in the inset of Fig. 2 where a size distribution generated by a hard sphere molecular dynamics simulation of an aerosol undergoing simultaneous nucleation and coagulation growth is shown. This two-dimensional simulation was carried out for 63 μs with a nucleation rate of $3\times10^5$ nuclei/pulse, in a 35 $\mu m^2$ area containing $4\times10^5$ background gas molecules [14]. A critical nucleus size of 1 nm was used and particles were allowed to coagulate and accumulate in the simulation domain. The inset of Fig. 2 shows that pulsed nucleation accompanied by accumulation leads to bimodal size distributions in qualitative agreement with our measured size distributions.

## 3. Gas Phase Nanoparticle Dynamics Model

A population of gas-suspended nanoparticles undergoing simultaneous nucleation and coagulation can be characterized by the time-dependent number concentration $N_k(t)$ governed by the discrete aerosol general dynamic equation [15]

$$\frac{dN_k}{dt} = \tfrac{1}{2}\sum_{j=1}^{k-1}\beta_{j,k-j}N_jN_{k-j} - N_k\sum_{j=1}^{\infty}\beta_{k,j}N_j + I_0(t)\delta_{k,1} \qquad (1)$$

where the index *k* represents the number of "monomers" contained in a particle, $I_0(t)$ is the nucleation rate of "monomers," and $\beta_{i,j}$ is the coagulation coefficient. When Brownian diffusion and Coulomb interactions are both at play, $\beta_{i,j}$ may be written as

$$\beta_{i,j} = 4\pi\left(R_{pi} + R_{pj}\right)\left(D_i + D_j\right)\gamma\left(\frac{n^{(l)}W_{(l)}^{-1} + n^{(u)}W_{(u)}^{-1}}{n^{(l)} + n^{(u)}}\right). \tag{2}$$

where $R_{pi}$ and $R_{pj}$ denote the radii of the colliding particles while $D_i$ and $D_j$ represent the corresponding particle diffusion coefficients. The last term in parentheses is the correction to pure Brownian coagulation that results from Coulomb interactions. It represents a weighted average of two opposing effects: (i) the *inhibition* of coagulation due to the presence of particles of "like" charge in the aerosol, accounted for by the coefficient $W_{(l)}^{-1}$, and (ii) the *enhancement* of coagulation due to particles of "unlike" charge, given by $W_{(u)}^{-1}$. The concentrations $n^{(l)}$ and $n^{(u)}$ represent the number of particle pairs with "like" and "unlike" charge, respectively. The coefficients $W_{(l)}^{-1}$ and $W_{(u)}^{-1}$ are found in the calculation of the inter-particle flux responsible for coagulation when both Brownian diffusion and Coulomb interactions are considered and are given by [15]

$$W_c^{-1} = \frac{\kappa}{e^{\kappa} - 1}, \tag{3}$$

where $\kappa = q_i q_j / \varepsilon(R_{pi} + R_{pj})kT$, with $q_i$ and $q_j$ representing the charge of the colliding particles and $\varepsilon$ the dielectric constant of the medium. $\kappa$ can be interpreted as the ratio of the electrostatic potential energy at particle contact to the thermal energy *kT*. Therefore a positive $\kappa$ corresponds to "like" charges, while a negative $\kappa$ represents "unlike" charges.

Since the aerosol in our system clearly develops a bimodal size distribution due to simultaneous operation of nucleation and accumulation processes, an approximate solution to Eq. (1) can be obtained using a simple bimodal model that represents the particle size distribution by two discrete monodisperse modes $N_1(t)$ (Mode 1) and $N_2(t)$ (Mode 2) [16]. In this approximation Mode 1 and Mode 2 are monodisperse and only three coagulation processes need to be considered, the coagulation between Mode 1 particles, the coagulation between Mode 2 particles, and the coagulation between Mode 1 and Mode 2 particles. Hence Eq. (1) simplifies to

$$\frac{dN_1}{dt} = -\frac{1}{2}\beta_{11}N_1^2\left(\frac{r}{r-1}\right) - \beta_{12}N_1N_2 + I_0(t), \tag{4}$$

$$\frac{dN_2}{dt} = \frac{1}{2}\beta_{11}N_1^2\left(\frac{1}{r-1}\right) - \frac{1}{2}\beta_{22}N_2N_2, \tag{5}$$

where coagulation coefficients are expressed as $\beta_{11}$, $\beta_{22}$, and $\beta_{12}$. Newly coagulated particles are statistically apportioned to Modes 1 and 2 according to the factors $r/(r-1)$ and $1/(r-1)$, where $r = v_2/v_1$ represents the volume ratio of Mode 2-particles to Mode 1-particles. For example, when two particles in Mode 1 collide, the resultant particle has a volume of $2v_1$. If the average volume of Mode 2 particles is $2v_1$ there is no need to apportion the resultant particle. However, since this is usually not the case, the resultant particle must be apportioned according to the particle volume ratio, which is $(r-2)/(r-1)$ to Mode 1 and $1/(r-1)$ for Mode 2. Knowledge of $r(t)$ requires additional equations for $v_1(t)$ and $v_2(t)$. These can be obtained by writing the equations for the total particle volume in Modes 1 and 2, i.e.,

$$\frac{dV_1}{dt} = -\frac{dV_2}{dt} + I_0(t)v_1(t), \tag{6}$$

$$\frac{dV_2}{dt} = \frac{1}{2}\beta_{11}N_1^2\left(\frac{r}{r-1}\right)v_1(t) + \beta_{12}N_1N_2v_1(t), \tag{7}$$

where $V_1(t) = v_1(t)N_1(t)$ and $V_2(t) = r(t)v_1(t)N_1(t)$. Changes in $v_1(t)$ may be accounted for by

$$\frac{dv_1}{dt} = \frac{1}{N_1}\frac{dV_1}{dt} - \frac{v_1}{N_1}\frac{dN_1}{dt}, \tag{8}$$

Equations (4-8) represent a system of independent equations that can be solved for the five unknown functions of interest $N_1(t)$, $N_2(t)$, $V_1(t)$, $V_2(t)$, and $v_1(t)$. A solution of this system provides a description of our nanoparticle population.

The formation of the ZnO aerosol probed in our experiments may be regarded as a two-phase process [13]. In an initial stage, nanoparticles nucleate from gas phase species as the hot plasma is quenched in contact with the background gas at the expansion front of the plume. The high concentration of nuclei in this region leads to a rapid onset of coagulation growth. As the aerosol is transported away from the plume, a second stage follows where nucleation ceases and coagulation growth dictates aerosol evolution. The duration of the initial stage can be estimated by dividing the thickness of the boundary layer, where the vaporized atoms are quenched and nucleate, by the average streaming velocity of atoms in the plume. Based on plume diagnostics measurements under similar experimental conditions, the thickness of the boundary layer and the average streaming velocity was estimated to be 1.0 mm [17] and 5.0 × $10^4$ cm/s [18], respectively, at atmospheric pressure. Using the values above, we estimate this initial stage to last for a time of approximately $\tau = 2\,\mu$s. For $t > \tau$ the aerosol evolves only due to coagulation until $t = \tau_{res}$, the residence time of the system between the plume region and the point of

neutralization. In our configuration $\tau_{res} \approx 15$ s. We have modeled this process by solving Eqs. (4-8) in two steps: In the initial stage ($0 < t < \tau$) the nucleation rate is set to a constant value $I_0$. Since Mode 1 here represents nucleation, the volume of the individual particles $v_1$ is also fixed to the volume of the critical nuclei while Mode 2 is allowed to grow as a result of coagulation. In the second stage ($\tau < t < \tau_{res}$) the nucleation rate is set to zero while both Mode 1 and Mode 2 are allowed to develop as a function of time due to coagulation.

Figure 3 shows a comparison between the measured diameters of Modes 1 and 2 and those predicted by the model of Eqs. (4-8) assuming a critical nucleus diameter of 1.2–3.6 nm [19] and a nucleation rate $I_0 = 6.0 \times 10^{16}$ cm$^{-3}$. Under the condition of aerosol neutrality, the model predicts diameters that are significantly larger and number concentrations that are significantly lower than those observed experimentally (not shown in figure). This suggests that electrostatic effects retard coagulation. By adjusting the ratios $n^{(l)}/n^{(u)}$, which quantify by how much the aerosol charge state deviates from neutrality, the model predicts diameters and concentrations that approach those measured. The best match between the model and the experiment is obtained for values of $n^{(l)}/n^{(u)}$ equal to 400, 160, and 10 for $\beta_{11}$, $\beta_{12}$, and $\beta_{22}$, respectively. Results are particularly sensitive to the ratio $n^{(l)}/n^{(u)}$ for inter-mode coagulation ($\beta_{12}$) as shown in Fig. 3. A value for $n^{(l)}/n^{(u)}$ of 350 leads to a decrease in the final diameter of Mode 2 from 47 nm to close to 39 nm which represents the experimental value. The number concentrations of nanoparticle population of Mode 1 and Mode 2 ware found to be consistent with the DMA measurement results.

## 4. Conclusion

Measured bimodal size distributions of laser-generated ZnO nanoparticle populations generated due to simultaneous nucleation and coagulation were compared with a simple particle dynamics model. Model results can only be matched with experiments if significant electrostatic effects are considered in the description of the problem.


## ACKNOWLEDGEMENTS

This research was supported by grants from the National Science Foundation (Research Experiences for Undergraduates site at the University of Alabama at Birmingham (UAB), DMR-0243640; Major Research Instrumentation, DMR-0116098) and the National Aeronautics and Space Administration (NASA/EPSCoR, NCC5-580). M. M. acknowledges support from the UAB Graduate Assistant Fellowship Program.

**Figure Captions**

Figure1: Schematic of the experimental apparatus used for measurements of the ZnO aerosol. The data points in the inset correspond to a typical bimodal size distribution measured during ZnO ablation. The data is well represented by a superposition of two log-normal functions with geometric mean diameters of 14 and 39 nm and geometric standard deviations of $\sigma_g$ = 1.55 and 1.65, respectively.

Figure 2: Effect of laser pulse energy on the relative intensities of the two modes of the size distribution. The inset shows a qualitatively similar bimodal distribution generated in a hard sphere molecular dynamics simulation accounting for simultaneous particle nucleation, coagulation, and accumulation.

Figure 3: (a) Number concentration of Mode 1 and Mode 2 particles with changing like- and unlike- particle ratio. (b) Mobility diameter of Mode 1 and Mode 2 particles with changing like- and unlike- particle ratio.

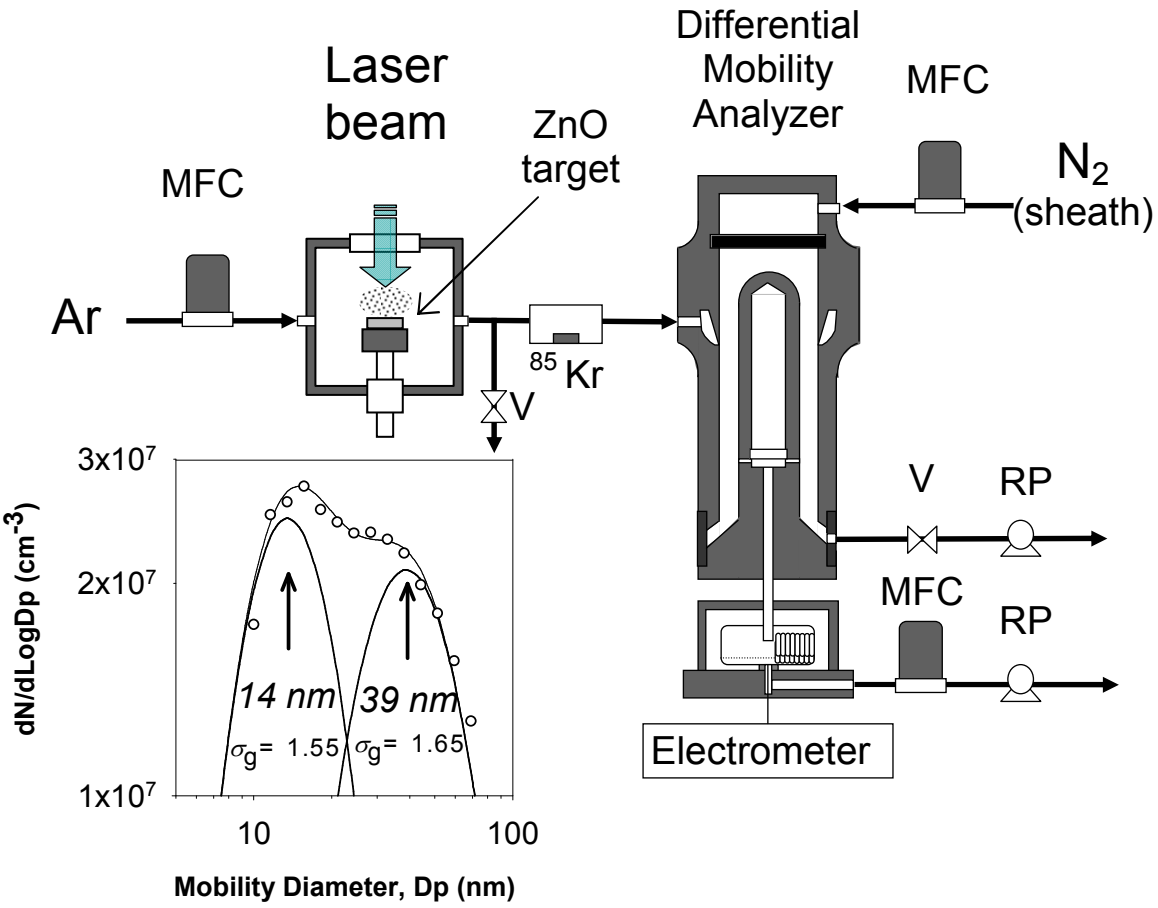


Fig. 1 - Matsumura et al.

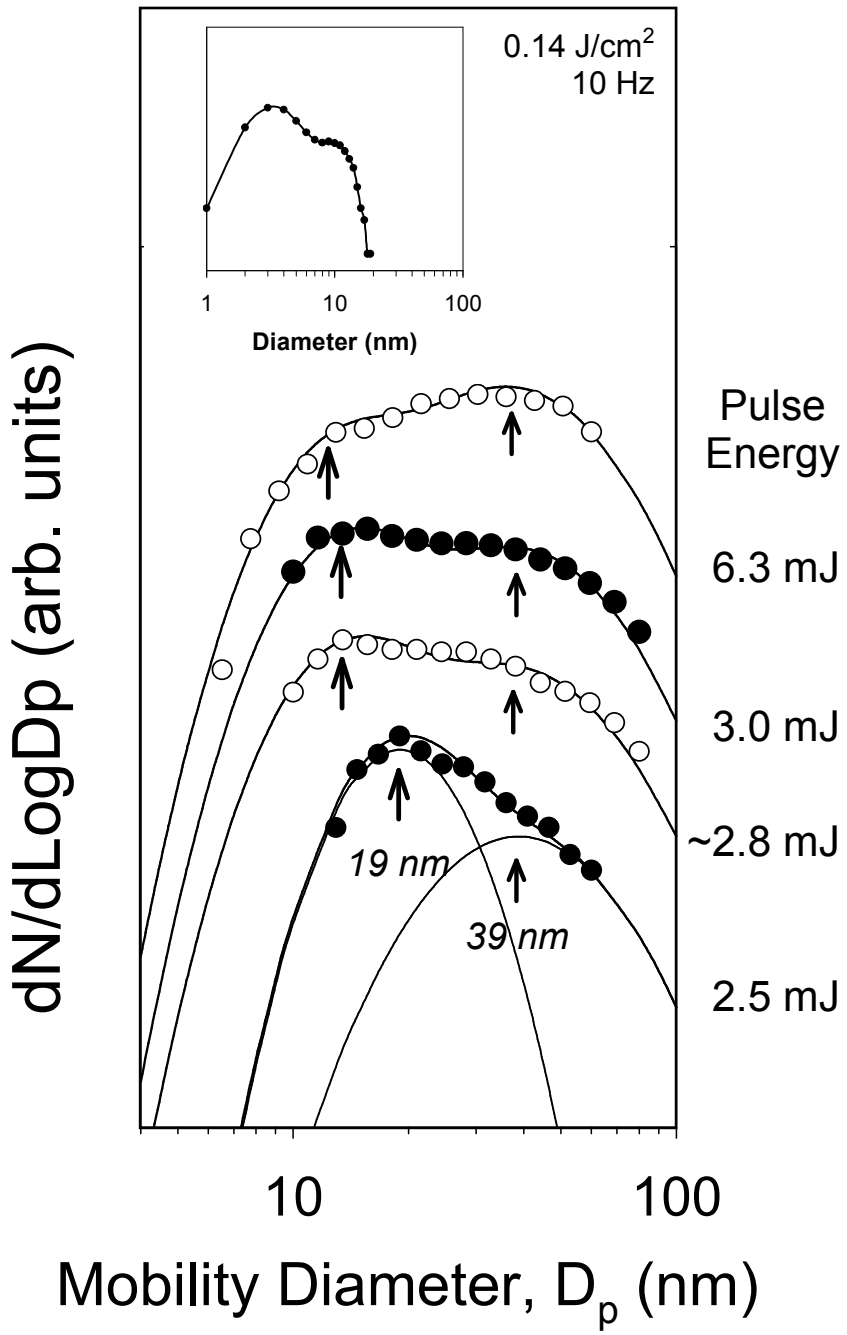


Fig. 2 - Matsumura et al.

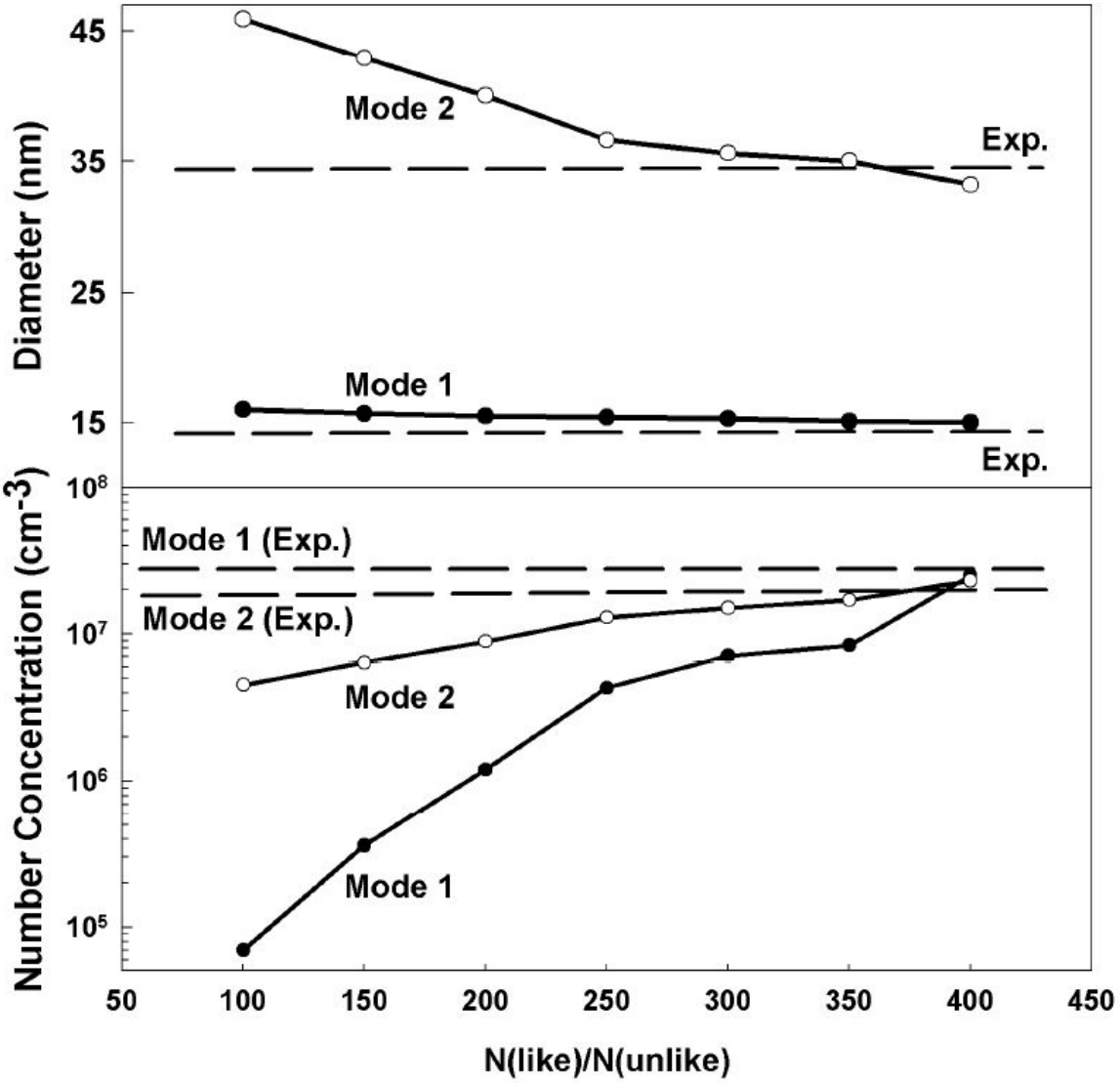


Fig. 3 - Matsumura et al.

## REFERENCES


1. W. Q. Peng, S. C. Qu, G. W. Cong, and Z. G. Wang, "Synthesis and temperature-dependent near-band-edge emission of chain-like Mg-doped ZnO nanoparticles", Appl. Phys. Lett., **88** (2006) 101902.
2. H. Zeng, W. Cai, B. Cao, J. Hu, Y. Li, and P Liu, "Surface optical phonon Raman scattering in Zn/ZnO core-shell structured nanoparticles" Appl. Phys. Lett., **88** (2006) 181905.
3. H. Amekura, O. A. Plaksin, M. Yoshitake, Y. Takeda, N. Kishimoto, and Ch. Buchal, "Atomic force microscopy and x-ray photoelectron spectroscopy studies of ZnO nanoparticles on SiO2 fabricated by ion implantation and thermal oxidation", Appl. Phys. Lett., **89** (2006) 023115.
4. C. Yuen, S.F. Yu, S. P. Lau, G. C. K. Chen, "Design and fabrication of ZnO light-emitting devices using filtered cathodic vacuum arc technique", *J. Crystal Growth*, **287** (2006) 204.
5. F. Verbakel, S. C. J. Meskers, and R. A. J. Janssen, "Electronic memory effects in diodes from a zinc oxide nanoparticle-polystyrene hybrid material", Appl. Phys. Lett., **89** (2006) 102103.
6. A. Talbi, F. Sarry, M. Elhakiki, L. Brizoual, O. Elmazria, P. Nicolay, and P. Alnot, "ZnO/quartz structure potentiality for surface acoustic wave pressure sensor", *Sensors and actuators. A, Physical.* **128**, (2006): 78.
7. S. H. Lee, S.S. Lee, J. J. Choi, J. U. Jeon, and K. Ro, "Part 2 - Section 8 - Microsensor/MEMS/Nano - Fabrication of a High-Aspect-Ratio Nano Tip Integrated Micro Cantilever with a ZnO Piezoelectric Actuator", *Key Eng. Mater.* **270**, (2004) 1095.
8. S. W. Kim, T. Kotani, M. Ueda, S. Fujita, and S. Fujita, "Selective formation of ZnO nanodots on nanopatterned substrates by metalorganic chemical vapor deposition", Appl. Phys. Lett., **83** (2003) 3593.
9. R. Viswanatha, S. Sapra, B. Satpati, P.V. Satyam, B. N. Dev, D. D. Sarma, "Understanding the quantum size effects in ZnO nanocrystals", J. Mater. Chem. **16** (2004) 661.
10. T. Tani, L. Madler, S. E. Pratsinis, "Homogeneous ZnO Nanoparticles by Flame Spray Pyrolysis" J. Nanopart. Res, **4** (2002) 337.
11. S. Polarz, A. Roy, M. Merz, S. Halm, D. Schoröder, L. Schneider, G. Bacher, F. E. Kruis, and M. Driess, "Chemical vapor synthesis of size-selected zinc oxide nanoparticles", Small, **5** (2005) 540.
12. H. Zeng, W. Cai, J. Hu, G. Duan, P. Liu, and Y. Li, "Violet photoluminescence from shell layer of Zn/ZnO core-shell nanoparticles induced by laser ablation", Appl. Phys. Lett., **88** (2006) 171910.
13. R.P. Camata, M. Hirasawa, K. Okuyama, and K. Takeuchi, "Observation of aerosol formation during laser ablation using a low-pressure differential mobility analyzer", J. Aerosol Sci., **31** (2000) 391.
14. See for example, A. Donev, S. Torquato, F. H. Stillinger, Neighbor List Collision-Driven Molecular Dynamics Simulation for Nonspherical Hard Particles. I. Algorithmic Details. J. Comput. Phys., 202, 737 (2005).

15. J. H. Seinfeld, “Atmospheric Chemistry and Physics of Air Pollution” A Wiley Int. Pub.
16. J. I. Jeong, and M. Choi, “A simple bimodal model for the evolution of non-spherical particles undergoing nucleation, coagulation and coalescence”, *Aerosol Sci.*, **34** (2003) 965.
17. A. K. Sharma and R. K. “Plume dynamics of laser-produced aluminum plasma in ambient nitrogen”, Appl. Surf. Sci., 243 (2005) 68.
18. R. M. Gilgenback and P. L. G. Ventzek, “Dynamics of excimer laser-ablated aluminum neutral atom plume measured by dye laser resonance absorption photography”, Appl. Phys. Lett., 58 (1991) 1597.
19. J. D. Bryan, D. A. Schwartz, and D. R. Gamelin, “The influence of dopants on the nucleation of semiconductor nanocrystals from homogeneous solution”, J. Nanoscience and Nanotech., 5 (2005) 1472.